University of British Columbia - Okanagan

Kelowna BC, Canada

PHYS 331 Term 1 2023W

October 2023

Investigating Wireless Power Transfer in Air, Pure Water, and Salt Water

Skyler Alderson and [redacted]

Abstract

Using a pair of Loop Gap Resonators equipped with a coupling loop inside each and a Vector Network Analyzer system, the transmission efficiency from one resonator to the other resonator was measured. This was done using reflection and transmission coefficients determined by the Vector Network Analyzer. These measurements were performed at varying separation distances between the resonators to observe how the transmission efficiency changes with distance. The transmissions were measured through three media: air, de-ionized water, and salt water. A metric of a -3 dB change in amplitude was used to compare power transfer efficiency. This metric occurred at 11.4 ± 0.2 cm in air, 17.0 ± 0.2 cm in deionized water, and less than 2 cm in salt water.

1 Introduction

1.1 History and Motivation

Over a century ago, Wireless Power Transfer (WPT) was first pioneered by Nikola Tesla (1856-1943). He extended on the work of Heinrich Hertz (1857-1894) and was simultaneously working on radio technology that Guglielmo Marconi (1874-1937) got credit for and developing WPT systems. He developed and demonstrated a set of principles for inductive nonradiative transfer. During the 1890s in his South Fifth Avenue laboratory in New York City, he demonstrated nonradiative transfer using a single loop coil that ran around the entire room driven by an oscillator and a three-foot-tall receiving coil on wheels. The receiving device could be moved to anywhere in the room and light bulbs were able to be switched on in an outlet mounted to the top of the unit. Friends and journalists were able to visit and witness demonstrations of powering various light bulbs from across the room. [1] This transfer is known as Inductive Power Transfer (IPT). The three principles for which Tesla is credited are:

1. There is inductive coupling between a driving circuit and a working circuit,
2. Both circuits are frequency-tuned for mutual resonance, and
3. The use of a capacitor in an additional circuit connected to the driving circuit to compensate any power reductions. [2]

Based on these principles, it became possible to transfer power over short and medium ranges. Since 2008, the Wireless Power Consortium established the standards for battery charging through inductive and resonant technologies. This is now used with Qi chargers that use a coil in a power transmission pad and a coil in a receiving device. These devices are mobile phones, tablets, smartwatches, and toothbrushes [3]. Another important application for IPT is to charge medical implants without needing to perform open surgery. The power can be transferred through the patient's skin and flesh such that their implant can be recharged [2]. With the accelerating emergence of the Electric Vehicle (EV) and growing concerns over driving range per battery charge, there is research and development on the idea of the Moving Field Inductive Power Transfer (MFIPT) system. This consists of a series of driving coils controlled by a complex switching system built into the road which charges the EV while it is traveling [3]. For the longest stretches of highway where charging stations are scarce, regular intervals of a few kilometers of road can be integrated with MFIPT technology to give the EV a boost in charge, improving its driving range and ability to reach a charging station.

Tesla's ultimate goal was to construct a global transmission system that broadcasts both intelligible information signals and energy. He is quoted to have predicted the smartphone. He obtained financial backing from J.P. Morgan and built the iconic Wardenclyffe tower laboratory. Marconi was proving more successful in transmitting information across the Atlantic while Telsa was making slow progress and asking for more funding. Eventually, Morgan had to focus on other pressing business ventures. Soon, Marconi was transmitting radio signals across the Atlantic and Morgan had stopped funding Tesla's work. Tesla was focused on transmitting energy and it was possible that Tesla would let people have wireless energy for free even if it would not be profitable for Morgan. Tesla struggled to find funding from other sources and suffered a mental breakdown; the Wardenclyffe Tower never succeeded in transmitting energy. [1]

1.2 Experimental Apparatus

The following experiment is based on the use of the Loop-Gap Resonator (LGR). An LGR has a simple design that combines all the effects of a circuit with an inductor, resistor, and capacitor (LRC circuit). An LRG consists of a thick-walled pipe with a slot cut out along the side. Figure 1a is a depiction of an LGR. The LGR behaves like an LRC circuit due to the cylindrical shape behaving like an inductor, the slot cutout behaving like a capacitor, and the conductive metal of the LGR has an overall resistance. This style of LGR is also known as a split-ring resonator. Generally, inductive power transfer has been done by tuning a pair of LRC circuits to resonance. At resonance, power can be transferred from one circuit, or one LGR, to the other.

The resonant tuning in each LGR is accomplished by use of a coupling loop positioned inside the LGR. The coupling loop is soldered to a copper rod that goes up through the top of the LGR and terminates at about 20cm above the LGR unit. There is no contact between this copper rod and the LGR itself. At the top of the copper rod is a coaxial cable connection. By twisting the copper rod, the coupling loop is rotated which in turn changes the resonant transmission. Figure 1b shows the complete LGR assembly.

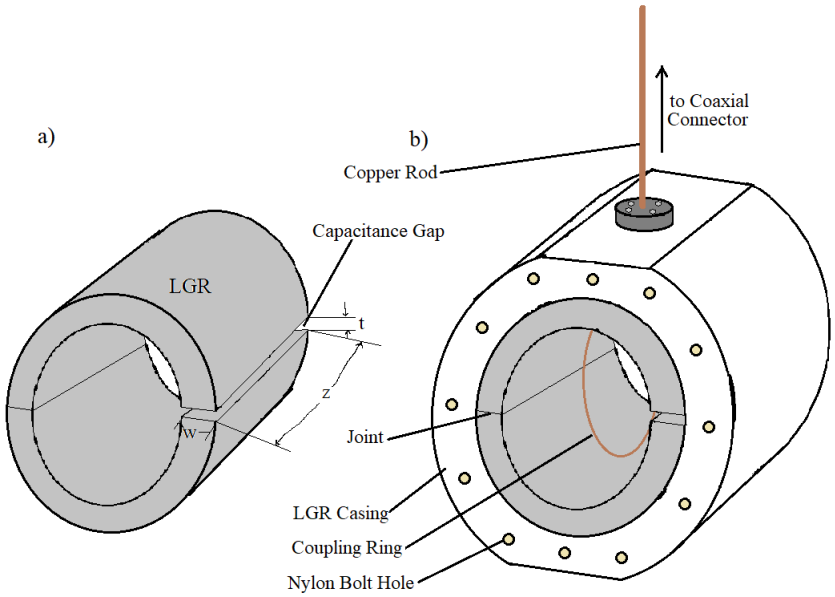

Figure 1: LGR Assembly. Part a) shows the LGR itself with relevant dimensions labeled, which can be used to determine the resistance, inductance, and capacitance of the LGR. Part b) shows the LGR within its casing and the coupling loop built into it. The full assembly in part b) is used for the experiment.

The data collected is done via a Vector Network Analyzer (VNA). A coaxial cable connects the aforementioned copper rod to the VNA console. Since there are two LGRs, there is a coaxial cable running from each LGR and they feed independent channel ports on the VNA console. The VNA console is connected to the computer with software to display the plot readings. All readings are measured in decibels as functions of frequency.

The LGRs are set on a styrofoam pad next to a ruler with inches marked on it. The ruler is used to measure the LGR separation. For in-water testing, each LGR has a set of plexiglass plates with rubber gaskets to seal off each end. The plates are fastened down by nylon screws. A large bin is used to hold water for later parts of the experiment. In the bin, there is a raised platform with a plastic ruler mounted to it. Likewise, to open air, the ruler is used to determine separation distance. Figure 2 shows the open-air setup.

1.3 Vector Network Analyzer (VNA) Theory Overview

The equivalent circuit schematic diagram for the coaxial lines connected to the VNA Console is given in Figure 3. There is a source impedance of the transmitting circuit Z_S, and the load impedance of the receiving circuit Z_L, and the transmitting circuit is driven by an AC source. Each a term represents a waveform signal transmitted to the other LGR, while each b term represents a waveform signal reflected back to each LGR. The index number for each a or b term corresponds to the channel number it is plugged into.

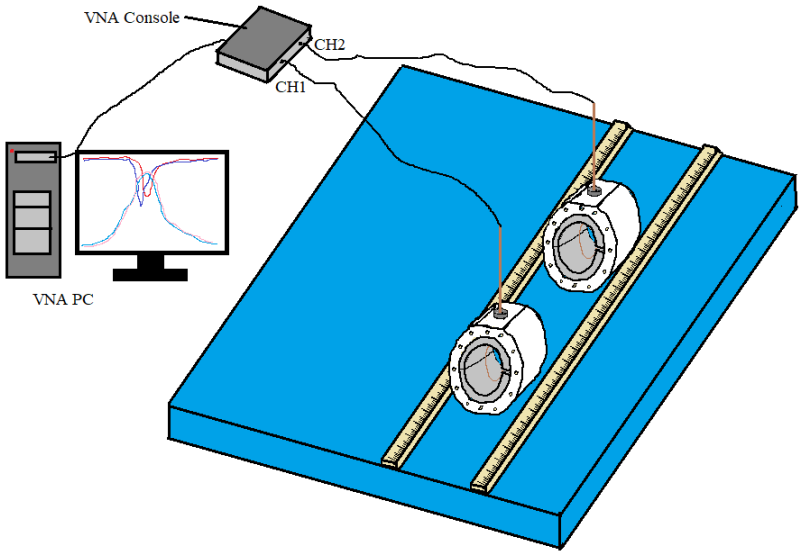

Figure 2: Both LGRs are in position along the rulers. Coaxial cables connect the LGRs to the VNA console. The VNA console is connected to the PC via USB where reflection and transmission coefficients are plotted as a function of frequency.

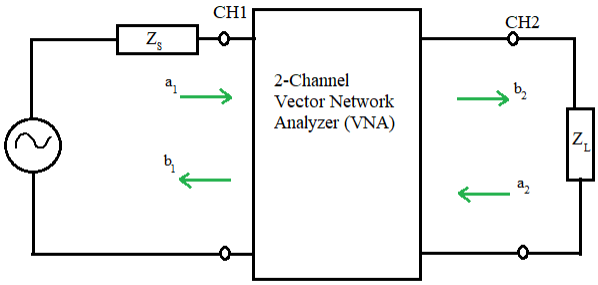

Figure 3: An equivalent circuit diagram for the VNA. An alternating signal is generated first through CH1 and then through CH2. The two impedances, Z_S and Z_L, each represent an LGR.

The vector network relation is given by,

$$\begin{pmatrix} b_1 \\ b_2 \end{pmatrix} = \begin{pmatrix} S_{11} S_{12} \\ S_{21} S_{22} \end{pmatrix} \begin{pmatrix} a_1 \\ a_2 \end{pmatrix}. \tag{1}$$

The resultant reflected power vector is a linear transformation of the S-matrix and the resultant transmitted power vector. The VNA analyzes this network of vectors. The b_2 component can be extracted and expressed by,

$$b_2 = a_1 S_{21} + a_2 S_{22}. \tag{2}$$

By the maximum power transfer theorem, $Z_S = Z_L$, and $a_2 = 0$. The S_{21} parameter can then be expressed as,

$$S_{21} = b_2 / a_1. \tag{3}$$

The reader can notice that each S-parameter can be defined this way by dividing the b component by the corresponding a component and keeping the indices in the same order. It is the S_{21} parameter that we want to maximize as it represents the amplitude of the transmitted wave while we want to minimize reflection terms like S_{11}. Since our LGRs are identical, the S_{12} and S_{21} curves are equivalent. [2]

1.4 Power Dissipation Through a Medium via Current Loops

Wandinger et. all [4] create an approximate formula for the power dissipated δP through a conducting medium. They assume there is a magnetic field with maximum amplitude $B_0(x)$ oscillating at the resonant frequency ω_0 of an LGR through a medium of uniform conductivity σ. If r_0 is the radius of the LGR bore and r is the distance from the x-axis to a point, then the average power dissipated over a time span of one period is

$$\langle dP \rangle = \left\langle \int_{r=0}^{r_0} \delta P \right\rangle = \frac{\pi}{16} r_0^4 \sigma \omega_0^2 B_0^2(x) dx. \tag{4}$$

This power is dissipated by ions moving in a circular motion through the medium around magnetic field lines. While equation (4) has not been integrated, it allows for qualitative reasoning on strategies to minimize power dissipation. One such strategy, as seen in Experimental Methods, is to artificially limit the current loop size by introducing a dividing grid in order to limit the dominating r_0^4 term in (4).

2 Experimental Methods

We first placed the two LGRs an arbitrary distance apart and ensured that they were parallel to one another, with an open face pointing towards the other LGR. We measured the distance between the two faces of the LGRs. Then, we adjusted the angular orientation of each LRG's coupling loop about the copper rod until we found the peak S_{21} for that distance. After recording the values for frequency and amplitude of the transmitted and reflected waves for the resonant frequency, we moved the LGRs to a new position and began the procedure again. We began each set of trials with a coarse scan with distance steps of about 5 cm. Then, we would perform a fine scan around -3 dB, which we define as the critical distance. We would also take measurements in sparse regions to ensure the shape of the curve could be clearly resolved. In the case when there was double resonance, which occurs when the separation between the LGRs is small, we used the S_{21} peak with a greater amplitude. We continued to take measurements at varying distances until a plot of peak S_{21} versus separation distance clearly resolved the shape and critical distance.

The VNA software collects signals from the VNA Console, processes it and produces plot curves. There are four curves in total and each represents the S-parameters in the S-matrix from equation (1). All curves are in amplitude (dB) as a function of frequency (MHz). The curves that represent the reflection S-parameters display as deep minima, and the curves that represent the transmission S-parameters display as high maxima. In order to maximize the efficiency of power transferred, we had to find the maximum amplitude of the transmission peaks (peak S_{12} or equivalently peak S_{21}); this roughly corresponds to maximizing the amplitude of the two deflection troughs, thus minimizing their values. We adjusted these troughs (troughs S_{11} and S_{22}), which itself adjusted the transmission curves, by changing the rotation of the coupling loops. We determined that we had optimized the transmission peak when we were unable to further improve the output of the VNA software.

While the LGRs should be identical and thus have the same resonant frequency for a given distance, we found that this was not the case. To account for this, we placed a small sheet of dielectric (Teflon) partially within the gap of one of the LGRs. By moving the sheet further into or out of the gap, we were able to adjust the capacitance of the LGR to match its pair.

At the beginning of each day of experimentation, the VNA was re-calibrated using its associated Magi-Cal calibration tool. This was done by removing the VNA's connections from the coupling loops and connecting them to the Magi-Cal device. It should be noted that a torque wrench was used for connecting and disconnecting the coaxial cables to ensure the cables were properly connected.

Before the LGRs were submerged in water, the open faces were sealed. In addition, a rubber ring seal around the base of the copper rod's connection to the LGR was re-greased. The tightness of the screws used to seal the LGRs affected the capacitance since it could change the distance of the capacitance gap, so the screws were adjusted until the capacitance of both LGRs was the same. We measured the conductivity of the water using a Beckman Conductivity Bridge. Once submerged in water, the procedure was the same.

When we changed our medium from de-ionized water to salt water by adding 20.06 g of sea salt, we waited until the salt had reached a dispersion equilibrium. Then, we remeasured the saltwater's conductivity. The saltwater trials otherwise proceeded the same as the previous trials.

In the next trial, we added two dividing grids with cell length 2.5 ± 0.2 cm and of equal depth between the LGRs, the grids placed flush against the LGRs' inner face. Similar to the previous trial, this proceeded in a medium of salt water. When the LGRs were moved to a new position, the grids were moved to remain flush against the LGRs. The trial otherwise proceeded the same as the saltwater trial.

3 Experimental Results

We found that a de-ionized water medium had the greatest critical distance at 17.0 ± 0.2 cm out of the three media used in this experiment. Air has a critical distance of 11.4 ± 0.2 cm and ionized water has a critical distance smaller than the minimum measurable distance of our apparatus. Figure 4 compares the peak S_{21} of each media as a function of separation distance.

The conductivity of the de-ionized water was found to be $(99 \pm 1) \times 10^{-5} \frac{1}{\Omega m}$. The conductivity of the salt water was found to be $(30 \pm 1) \times 10^{-3} \frac{1}{\Omega m}$. The conductivity of the media is proportional to the power dissipated through that media, as estimated be Wandinger et. all, which is consistent with the peak S_{21} for a particular distance of de-ionized water versus salt water, as seen in figure 4. [4]

We defined -3 dB to be the critical distance since it roughly corresponds to halving the amplitude of S_{21}. This provides a useful metric for the effective distance of power transfer efficiency. Beyond the critical distance, peak S_{21} appears to decrease linearly with distance. Prior to that distance, peak S_{21} decreases at a slower rate.

Our experimental apparatus was unable to obtain data with a distance smaller than the critical distance for the salt water trial. This is due in part to the coupling loops being in the centers of the LGRs so they could not be brought any closer together than the total length of a single LGR. As such, the minimum distance between the coupling loops was insufficient to offset the power dissipated in the medium, preventing a measurement with a separation smaller than the critical distance.

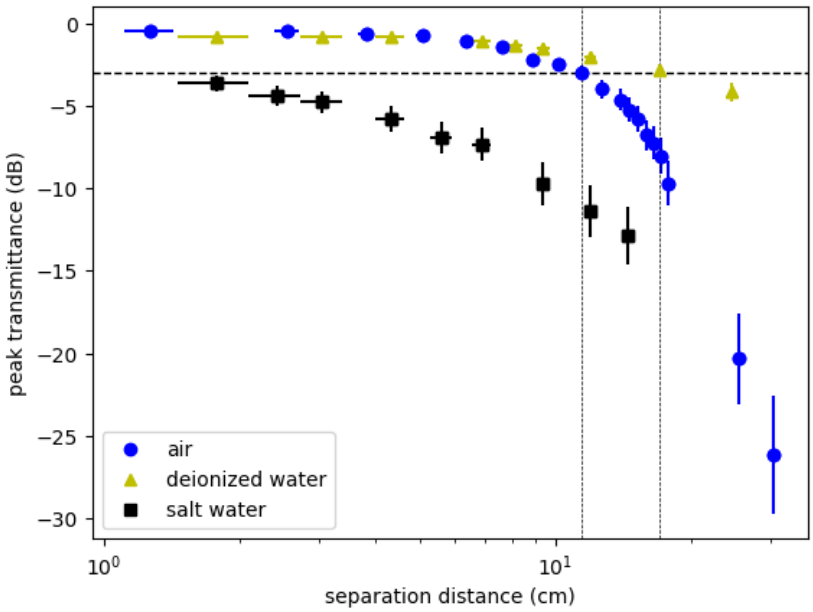

Figure 4: The peak transmittance as a function of distance for three different media: air, deionized water, and salt water. A horizontal dashed lines placed at -3 dB. The vertical dashed lines indicate where a trial crosses the critical distance. The greatest critical distance is associated with water, followed by air, and the smallest critical distance is associated with salt water.

As seen in figure 5, adding a dividing grid in the salt water medium had negligible effect. All data points in the salt water grid trial are within uncertainty of their respective data point at the same separation distance in the salt water trial without a grid. This study is unable to corroborate the results of Wandinger et. all relating to the impact of dividing grids on power dissipation through salt water. [4]

On figure 4, the leftmost data point for salt water occurs when the faces of the LGRs are touching, thus there is no salt water between them. This point reads at a distance of 1.8 ± 0.2 cm rather than 0 cm due to the sealing caps on the LGRs each having a thickness of 0.9 cm ± 2 cm. Even when this is the case, the point has a peak S_{21} of -3.6 ± 0.5 dB, nearly 3 db less than the corresponding point on water. If there

is no salt water between the LGRs and the peak S_{21} is significantly worse than trials in other media, then we can conclude media directly between the faces of the LGR does not significantly contribute to power dissipation. Thus, placing a dividing grid between the LGRs should not significantly affect the results of the trial. This analysis agrees with what is seen in figure 5, where the salt water grid trial data points are all within uncertainty of the salt water trial without a grid.

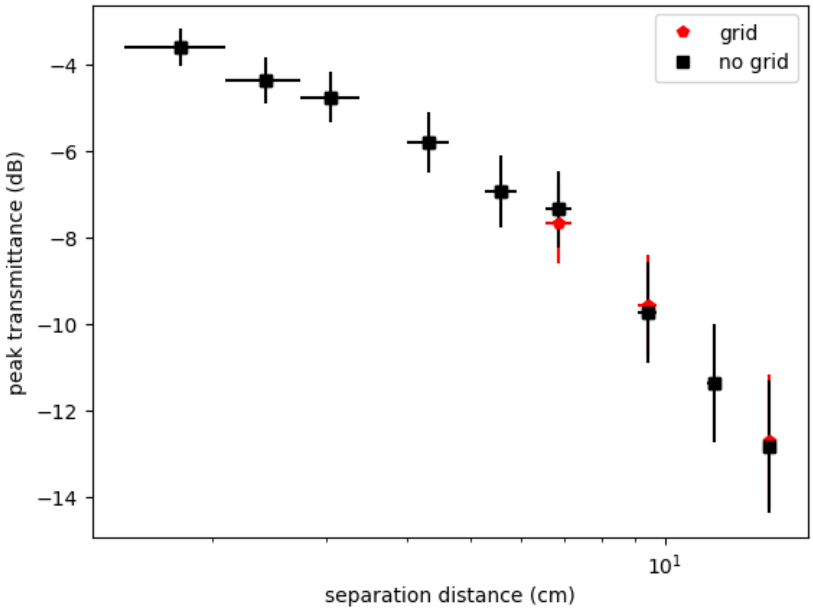

Figure 5: The peak transmittance as a function of distance for salt water with and without a dividing grid. The data points for the dividing grid trial are within the uncertainty of the maximum transmittance without a dividing grid.

The frequency at which peak S_{21} occurred approached a steady value as separation distance increased. At low separation, double resonance was present. Peak S_{21} tended to occur at the peak of greater frequency. As distance between the LGRs increased, the two peaks of double resonance approached a single peak with a frequency value roughly in the middle. This is consistent with what is seen in figure 6, the frequency of peak S_{12} as a function of separation distance. The initial data point for the air trial saw double resonance and its greatest peak was the one at lower frequency.

The uncertainty in peak S_{21} and its frequency were modeled by performing a series of measurements at a particular separation distance. After a measurement was taken, the orientation of the coupling loops and the separation distance were randomly altered so that another measurement at the previous particular separation distance could be taken. The random shuffling was done to ensure the full process of optimizing the peak S_{21} was observed for each measurement.

After this special trial was completed, the uncertainty in peak S_{21} and its frequency were obtained by taking the appropriate standard error, using it as that measurement's absolute uncertainty at that separation distance. This was converted to relative uncertainty so it could be applied to the other measurements of peak S_{21} and frequency.

This method was chosen as it was estimated that the relative uncertainty would be constant for all separation and for all media. The uncertainties associated with the VNA and the Beckman Conductivity Bridge were assumed to be negligible compared to the uncertainty associated with finding the optimal orientation of the conducting loops.

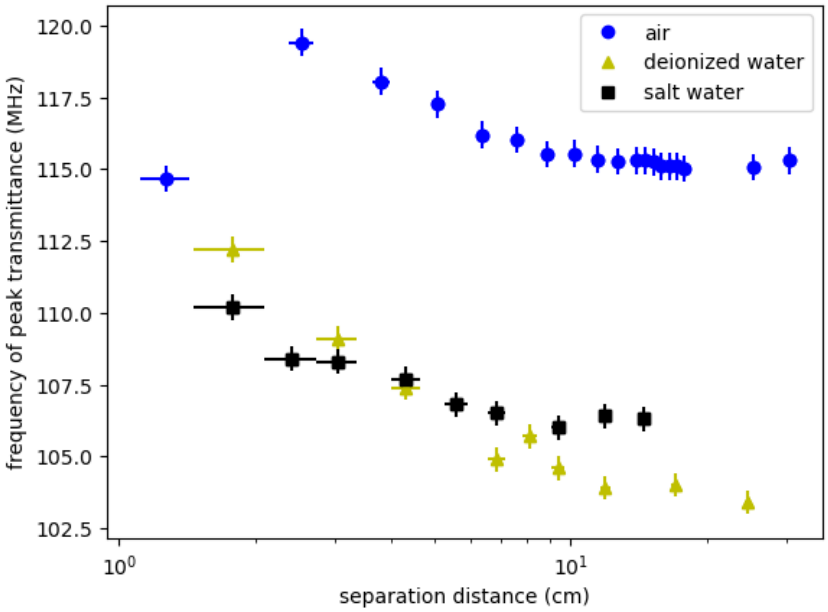

Figure 6: The frequency at which max transmittance occurs as a function of distance for three different media: air, deionized water, and salt water. At lower values for separation distance, the frequency tends to be greater. As separation distance increases, the frequency approaches a stable smaller value.

4 Conclusion

This experiment was able to successfully observe the relation between peak S_{21} and separation distance. The critical distance, defined as a change of -3 dB in peak S_{21}, was observed at 11.4 $\pm$ 0.2 cm in air, 17.0 $\pm$ 0.2 cm in deionized water, and less than 2 cm in salt water. At distances greater than the critical distance, peak S_{21} linearly decreases as separation distance increases.

We were unable to demonstrate that dividing grids placed between the LGRs decreased the power dissipation through an ionized medium, such as salt water. This could imply at least one of three things: that the circulation of ions about magnetic field lines are a negligible contributor to power dissipation in an ionized medium, that the cell dimensions chosen were too large thus unable to sufficiently restrict the circulation of ions, or the circulation of ions between the faces of the LGRs are negligible contributors compared to elsewhere in the medium. Improvements to this part of the experiment could include taking a greater number of measurements to see the dividing grid's effects both near and far from the critical distance, using dividing grids with various cell dimensions, and taking measurements with greater precision to be able to better resolve minute differences between the trials with and without a grid.

References

[1]W. Carlson, *Tesla: inventor of the electrical age* (Princeton University Press, 41 William Street, Princeton New Jersey, 08540, 2013), pp. 189–192.

[2]S. Hui, W. Zhong, and C. Lee, "A critical review of recent progress in mid-range wireless power transfer", English, IEEE Transactions On Power Electronics **29**, 4500–4511 (2014).

[3]S. Tahir and M. A. A. Rathore, "Medium range resonant inductive wireless power transfer", English, IEEE Electric Power an Energy Conference, 10.1109/EPEC48502.2020.9320031 (2020).

[4]D. R. J.N. Wandinger and J. Bobowski, "Inductive power transfer through saltwater", English, IEEE Electric Power an Energy Conference, 10.1109/ISEMA49699.2021.9508312 (2021).